

Slow dynamics from a nested hierarchy of frozen states

Vanja Marić,¹ Luka Paljk,¹ and Lenart Zadnik^{1,*}

¹*Department of Physics, Faculty of Mathematics and Physics,
University of Ljubljana, Jadranska 19, Ljubljana SI-1000, Slovenia*

We identify the mechanism of slow heterogeneous relaxation in quantum kinetically constrained models (KCMs) in which the potential energy strength is controlled by a coupling parameter. The regime of slow relaxation includes the large-coupling limit. By expanding around that limit, we reveal a *nested hierarchy* of states that remain frozen on time scales determined by powers of the coupling. The classification of such states, together with the evolution of their Krylov complexity, reveals that these time scales are related to the distance between the sites where facilitated dynamics is allowed by the kinetic constraint. While correlations within frozen states relax slowly and exhibit metastable plateaus that persist on time scales set by powers of the coupling parameter, the correlations in the rest of the states decay rapidly. We compute the plateau heights of correlations across all frozen states up to second-order corrections in the inverse coupling. Our results explain slow relaxation in quantum KCMs and elucidate dynamical heterogeneity by relating the relaxation times to the spatial separations between the active regions.

I. INTRODUCTION

The rapid progress of quantum technologies provides strong motivation for theoretical investigations into the mechanisms of slow relaxation in quantum many-body systems. A notable example is the growing interest in quantum kinetically constrained models (KCMs), whose classical analogs have historically played an important role in understanding dynamical slowdown and heterogeneity in structural glasses [1–4]. One of the appeals of quantum KCMs lies in the fact that they are experimentally accessible within Rydberg-atom platforms [5–12]. From a theorist’s standpoint, these systems are remarkable not only because they exhibit slow relaxation, but also because they support a rich variety of other exotic nonequilibrium phenomena. These range from Hilbert space fragmentation [13–17] and quantum many-body scars [18–21] to anomalous transport properties [22–25].

In this work we focus on the emergence of slow relaxation in quantum KCMs with a coupling parameter that tunes the strength of the potential energy. Specifically, we are interested in KCMs with two dynamical regimes, depending on the coupling strength: one exhibiting fast correlation decay and another where relaxation is markedly slowed, exhibiting metastable behavior [26–33]. The latter regime is associated with the emergence of a hierarchy of (prethermal) plateaus in the correlation functions. Such a dynamical slowdown has been addressed through the lens of emergent quantum many-body scars and enhanced kinetic constraints in the strong-coupling limit [30–32], as well as emergent (quasi)conserved quantities [34]. Here, we go beyond the strong-coupling limit by determining the microscopic mechanism that pinpoints the origin of *all* plateaus, thus explaining the entire hierarchy of relaxation times.

Specifically, we develop a framework within which both

the time scales and the heights of the plateaus can be determined. Based on the full large-coupling expansion of the Hamiltonian, our framework defines a nested hierarchy of computational-basis states that are preserved by a sequence of effective Hamiltonians governing the dynamics on different time scales. The latter scale exponentially with the distances between the active regions of space within which the dynamics is allowed under the kinetic constraint.

We will focus on the so-called XPX model [31, 35–37], but the results are applicable to other quantum KCMs. In support of this claim, we present additional results for the quantum version of the Fredrickson-Andersen model [2, 3, 38] in Appendix D.

II. SLOW DYNAMICS IN THE XPX MODEL

We consider the one-dimensional XPX model

$$H_{\text{XPX}} = \sum_{j=1}^L \sigma_j^x (1 - \sigma_j^z) \sigma_{j+1}^x + \Delta \sigma_j^z \quad (1)$$

with periodic boundary conditions. Here, σ_j^α , for $\alpha \in \{x, y, z\}$, are Pauli matrices in site j . The coupling parameter Δ controls the strength of the potential energy $V = \sum_{j=1}^L \sigma_j^z$. The kinetic term is constrained: spins \downarrow facilitate simultaneous spin flips on the neighboring sites.

Slow dynamics arises for $|\Delta| > 1$ [31] and it can be observed in the behavior of time-averaged correlation functions $\bar{c}_t(\mathbf{s}) = t^{-1} \int_0^t d\tau c_\tau(\mathbf{s})$, where

$$c_t(\mathbf{s}) := \frac{1}{L} \sum_{j=1}^L \langle \mathbf{s} | n_j(t) n_j(0) | \mathbf{s} \rangle. \quad (2)$$

Time averaging is employed to smooth out quantum coherences on short time scales. Here and in the following, $|\mathbf{s}\rangle \equiv |s_1 \dots s_L\rangle$ is a computational-basis state, with $s_j \in \{\uparrow, \downarrow\}$ labeling the eigenstates of σ_j^z , and

* lenart.zadnik@fmf.uni-lj.si

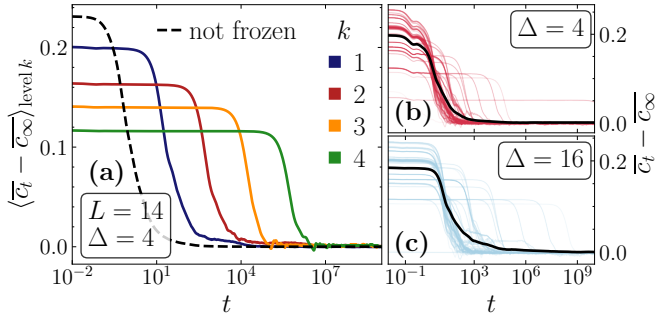


FIG. 1. **Slow relaxation in the XPX model.** Panel (a) shows a hierarchy of correlations $\bar{c}_t(s) = t^{-1} \int_0^t d\tau c_\tau(s)$, Eq. (2), averaged over the computational-basis states $|s\rangle$, frozen on time scales $t \sim \Delta^k$ (the so-called “level- k states”—see Fig. 2). The correlation function averaged over the rest of the states instead decays rapidly (dashed line). Panels (b) and (c) show correlations in all frozen states, as well as their average (black line). The initial plateau is more pronounced at larger Δ . In all plots the system size is $L = 14$.

$n_j(t) = e^{itH_{\text{XPX}}} n_j e^{-itH_{\text{XPX}}}$ is the Heisenberg time evolution of the site occupancy $n_j = (\mathbb{1} + \sigma_j^z)/2$. In Figs. 1(b) and 1(c) we show a selection of slowly relaxing correlation functions in the $|\Delta| > 1$ regime. For larger Δ , the first among the plateaus becomes more pronounced, persisting up to times $t \sim \Delta$ [31, 32]. In that (large-coupling) regime, the dynamics is governed by an effective Hamiltonian that is more constrained than H_{XPX} , its Hilbert space splitting into exponentially many dynamically disconnected sectors [13, 15, 16, 39, 40]. As a consequence, relaxation is suppressed up to times $t \sim \Delta$, around which corrections to the large-coupling limit become relevant, causing the plateau’s decay [15, 32, 39]. We will show that this decay occurs in stages and identify the precise mechanism behind such a hierarchical relaxation.

We will start with the key ingredient—the full large-coupling expansion of H_{XPX} . Successive truncations of this expansion yield kinetically constrained effective Hamiltonians that govern the dynamics on progressively longer time scales. Due to kinetic constraints, each one of

them has a set of computational-basis eigenstates, which we will classify and count. By tracking the evolution of their Krylov complexity [41, 42] under the full Hamiltonian H_{XPX} , we will show that such states are effectively frozen up to times that scale as powers of Δ . The plateaus appear only in the correlation functions in frozen states—they are shown in Fig. 1. We will calculate their heights up to $O(\Delta^{-2})$ corrections.

III. LARGE-COUPING EXPANSION

Our starting point is the recursive scheme of Ref. [43], which allows us to compute the large-coupling expansion up to any order in $1/\Delta$ (see Appendix A). It results in an anti-Hermitian $S = \sum_{n \geq 1} \Delta^{-n} S_n$ and a Hermitian $H_F = \sum_{n \geq 0} \Delta^{-n} H_{F,n}$, such that

$$H_{\text{XPX}} = e^{-S} H e^S, \quad H = H_F + \Delta V, \quad [H_F, V] = 0, \quad (3)$$

where $V = \sum_{j=1}^L \sigma_j^z$ is the potential energy. We will refer to H as the *effective Hamiltonian*, and to H_F as the *folded XPX model* [15, 16]. The name comes from the fact that the spectra of H_{XPX} and H_F are equivalent up to shifts that are integer multiples of Δ (the spectrum of H_{XPX} “folds” into the one of H_F). We also define truncations of the generator and of the effective Hamiltonian,

$$S^{(k)} := \sum_{n=1}^k \Delta^{-n} S_n, \quad H^{(k)} := \Delta V + \sum_{n=0}^{k-1} \Delta^{-n} H_{F,n}. \quad (4)$$

The first few orders in the expansion of H_F read

$$H_{F,0} = \sum_{j=1}^L \frac{\mathbb{1} - \sigma_j^z}{2} (\sigma_{j-1}^x \sigma_{j+1}^x + \sigma_{j-1}^y \sigma_{j+1}^y), \quad (5)$$

$$H_{F,1} = \sum_{j=1}^L \frac{\mathbb{1} - \sigma_{j-1}^z}{2} \sigma_j^z \frac{\mathbb{1} - \sigma_{j+1}^z}{2} (\sigma_{j-2}^+ \sigma_{j+2}^- + \text{H.c.}) + (\sigma_{j-1}^+ \sigma_j^- \sigma_{j+1}^+ \sigma_{j+2}^- + \text{H.c.}) + \sigma_j^z \frac{\mathbb{1} - \sigma_{j+1}^z}{2}, \quad (6)$$

and

$$\begin{aligned} H_{F,2} = & \sum_{j=1}^L \frac{3}{4} \left(\frac{\sigma_{j-2}^z + \sigma_{j+2}^z}{2} - \mathbb{1} \right) \left(\frac{\mathbb{1} - \sigma_j^z}{2} \right) (\sigma_{j-1}^+ \sigma_{j+1}^- + \text{H.c.}) + \frac{1}{2} \left(\frac{\mathbb{1} + \sigma_j^z}{2} \right) (\sigma_{j-2}^+ \sigma_{j-1}^- \sigma_{j+1}^+ \sigma_{j+2}^- + \text{H.c.}) \\ & - \frac{1}{2} \left(\frac{\mathbb{1} - \sigma_j^z}{2} \right) (\sigma_{j-2}^+ \sigma_{j-1}^- \sigma_{j+1}^- \sigma_{j+2}^+ + \text{H.c.}) + \frac{3}{4} \left(\frac{\mathbb{1} - \sigma_{j-1}^z}{2} \sigma_j^z \right) (\sigma_{j-2}^+ \sigma_{j+1}^- \sigma_{j+2}^+ \sigma_{j+3}^- + \text{H.c.}) \\ & + \frac{3}{4} \left(\sigma_{j+1}^z \frac{\mathbb{1} - \sigma_{j+2}^z}{2} \right) (\sigma_{j-2}^+ \sigma_{j-1}^- \sigma_j^+ \sigma_{j+3}^- + \text{H.c.}) + \frac{1}{4} \left(\sigma_{j+1}^z \frac{\mathbb{1} - \sigma_{j+2}^z}{2} \right) (\sigma_{j-2}^+ \sigma_{j-1}^+ \sigma_j^- \sigma_{j+3}^- + \text{H.c.}) \\ & + \frac{1}{4} \left(\frac{\mathbb{1} - \sigma_{j-1}^z}{2} \sigma_j^z \right) (\sigma_{j-2}^+ \sigma_{j+1}^+ \sigma_{j+2}^- \sigma_{j+3}^- + \text{H.c.}) + \left(\frac{\mathbb{1} - \sigma_{j-2}^z}{2} \sigma_{j-1}^z \frac{\mathbb{1} - \sigma_j^z}{2} \sigma_{j+1}^z \frac{\mathbb{1} - \sigma_{j+2}^z}{2} \right) (\sigma_{j-3}^+ \sigma_{j+3}^- + \text{H.c.}), \end{aligned} \quad (7)$$

where $\sigma_j^\pm = (\sigma_j^x \pm i\sigma_j^y)/2$. Additionally, we report the leading order of S :

$$S_1 = \frac{1}{2} \sum_{j=1}^L \frac{1-\sigma_j^z}{2} (\sigma_{j-1}^+ \sigma_{j+1}^+ - \sigma_{j-1}^- \sigma_{j+1}^-). \quad (8)$$

We note that $H_{F,0}$ is an integrable model, solved exactly in Refs. [15, 16, 40], while higher orders of the folded model, $H_{F,n}$, for $n \geq 1$, break integrability.

IV. NESTED HIERARCHY OF FROZEN STATES

Due to kinetic constraints in $H_{F,n}$, each truncation $H^{(k)}$ of the effective Hamiltonian possesses a set of computational-basis eigenstates referred to as *frozen states*¹:

$$\mathcal{C}_k := \{ |\mathbf{s}\rangle \equiv |s_1 \dots s_L\rangle \mid H^{(k)}|\mathbf{s}\rangle = \varepsilon(\mathbf{s})|\mathbf{s}\rangle \}. \quad (9)$$

From the way they are defined, such states do not depend on Δ . Since $H^{(k+1)} = H^{(k)} + \Delta^{-k} H_{F,k}$, according to Eq. (4), $H^{(k+1)}$ contains both the constrained hopping terms of $H_{F,k}$, as well as those already present within the lower-order truncation $H^{(k)}$. Higher-order truncations may allow for hopping processes within spin configurations that were frozen by the lower-order truncations. As a result $\mathcal{C}_{k+1} \subseteq \mathcal{C}_k$: only those frozen states of $H^{(k)}$ that remain eigenstates in the presence of additional constrained hopping processes described by $H_{F,k}$ are also frozen states of $H^{(k+1)}$. Frozen states can therefore be classified within a *nested hierarchy* of sets

$$\mathcal{C}_1 \supseteq \mathcal{C}_2 \supseteq \dots \supseteq \mathcal{C}_{k-1} \supseteq \mathcal{C}_k \supseteq \dots, \quad (10)$$

depicted in Fig. 2.

For illustration, consider first $H^{(1)} = \Delta V + H_{F,0}$, where the constraint comes from the leading-order folded model in Eq. (5). The only nontrivial hopping process allowed by the latter is $|\dots \uparrow\downarrow \dots\rangle \leftrightarrow |\dots \downarrow\uparrow \dots\rangle$: it requires the presence of a pair of neighboring \downarrow -spins. \mathcal{C}_1 therefore contains spin configurations in which subsequences $\downarrow\downarrow$ are forbidden. Additionally, according to the definition in Eq. (9), the “vacuum” state $|\downarrow\downarrow \dots \downarrow\rangle$, with all spins \downarrow , is trivially contained within \mathcal{C}_1 .

To identify \mathcal{C}_2 , i.e., the set of frozen states of $H^{(2)} = H^{(1)} + \Delta^{-1} H_{F,1}$, we have to inspect the kinetic constraints in Eq. (6). In particular, the off-diagonal terms of $H_{F,1}$ act nontrivially on configurations that contain any one of the following subsequences: $\downarrow\downarrow\downarrow$, $\downarrow\uparrow\downarrow$, $\downarrow\uparrow\downarrow\uparrow$, or $\uparrow\downarrow\uparrow\downarrow$ (some of them were frozen under $H^{(1)}$). Combined with the

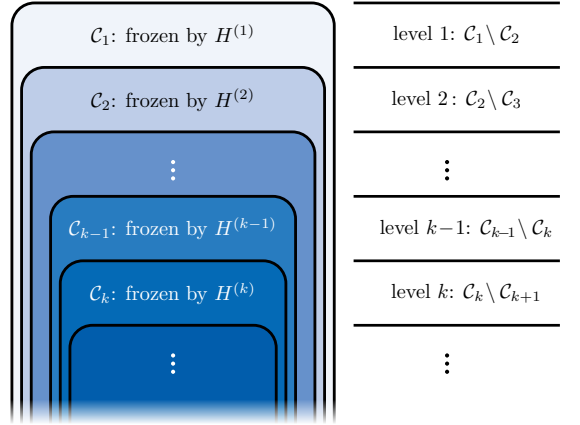


FIG. 2. **Nested hierarchy of states.** \mathcal{C}_k contains the states frozen by the truncation $H^{(k)}$ of the effective Hamiltonian H . Level- k states are those in \mathcal{C}_k that are only frozen by $H^{(\ell)}$ for $\ell \leq k$.

first-order frozen-state condition, which prohibits pairs of \downarrow -spins, we therefore have that \mathcal{C}_2 contains configurations without subsequences $\downarrow\downarrow$ or $\downarrow\uparrow\downarrow$.

The second correction, entering the truncation $H^{(3)} = H^{(2)} + \Delta^{-2} H_{F,2}$, is reported in Eq. (7). Inspecting the off-diagonal terms in that equation—in particular the second one—leads us to the conclusion that the configurations in \mathcal{C}_3 have no subsequences $\downarrow\downarrow$, $\uparrow\downarrow\downarrow$, or $\downarrow\uparrow\uparrow\downarrow$. The first two subsequences are forbidden since the state should be frozen under $H^{(2)}$, whereas the third subsequence is prohibited since the state should additionally be frozen under $H_{F,2}$.

More generally, the above observations suggest that, apart from the trivial vacuum state $|\downarrow\downarrow \dots \downarrow\rangle$,

\mathcal{C}_k contains spin configurations in which any two \downarrow -spins are separated by at least k \uparrow -spins.

In Appendix B we show that the number of such configurations is²

$$|\mathcal{C}_k| = 1 + \sum_{N=\lceil \frac{kL}{k+1} \rceil}^L \frac{L}{kN-(k-1)L} \binom{kN-(k-1)L}{L-N}. \quad (11)$$

It correctly reproduces the numerically computed numbers of frozen states, shown in Fig. 3(a). In Appendix B we also derive the large- L asymptotics of $|\mathcal{C}_k|$, obtaining

$$|\mathcal{C}_k| \sim \chi_k^L, \quad (12)$$

where χ_k is a solution of $\chi^k(\chi-1) = 1$. For $k = 1$ we have $\chi_1 = (1 + \sqrt{5})/2 \approx 1.618$, and for $k = 2$ the solution reads

¹ Since we demand the frozen states to be product states in the computational basis, they are also the eigenstates of the local density $h_j^{(k)}$, where $H^{(k)} = \sum_{j=1}^L h_j^{(k)}$.

² This formula is derived under the assumption that the system size L is larger than the number of adjacent sites acted upon by the local terms in $H^{(k)}$, i.e., $L > 2k + 1$.

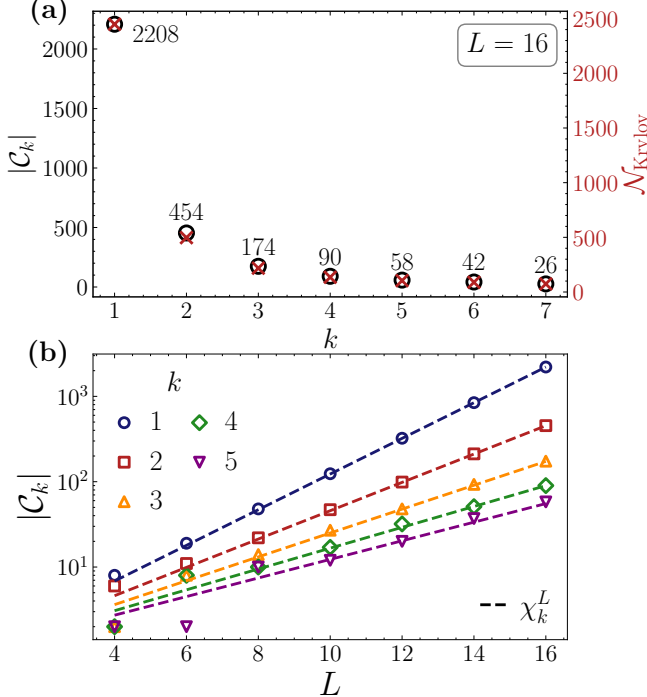


FIG. 3. **Frozen states and scaling of Krylov sectors.** Panel (a) shows the scaling of the number of frozen states $|\mathcal{C}_k|$ (black) and the number of Krylov sectors N_{Krylov} (red) with order k of the truncation, for system size $L = 16$. The values of $|\mathcal{C}_k|$ computed from Eq. (11) match the numerically computed ones shown in the plot. Panel (b) depicts the scaling of $|\mathcal{C}_k|$ with system size L for various k . The dashed lines show the asymptotic prediction from Eq. (12). In both panels the coupling was set to $\Delta = 4$.

$\chi_2 \approx 1.466$, both values matching the results previously obtained in Ref. [15]. The numerics confirms the scaling also for higher-order truncations—see Fig. 3(b).

We remark that the integrability of $H_{F,0}$ ensures the existence of stable quasiparticles [15, 16]. In frozen states belonging to \mathcal{C}_1 (apart from the trivial vacuum state), these quasiparticles are densely packed and immobile: the frozen states of $H_{F,0}$ are genuinely *jammed* [44, 45]. The leading order of the folded model H_F (and of the effective model H as well) moreover exhibits Hilbert space fragmentation, in which the dynamically disconnected (Krylov) sectors are labeled by specific jammed configurations [13, 15, 16]. While higher orders of the folded model are no longer integrable, they still seem to exhibit Hilbert space fragmentation, although to a lesser degree. Furthermore, we observe a correlation between the number of Krylov sectors and the number of frozen states in higher-order truncations of H —see Fig. 3(a): the scalings are the same up to a prefactor. This hints at a possible connection between the frozen states and the Hilbert space fragmentation also in higher orders of the effective Hamiltonian H . We leave this for future investigations. In the following we will instead demonstrate that the nested hierarchy of frozen states in Eq. (10) gives

rise to a hierarchy of time scales observed in dynamical correlation functions.

V. HIERARCHY OF TIME SCALES

Expanding the effective Hamiltonian in the time-evolution operator as $\exp(-itH) = \exp(-it\Delta V - i\sum_{n \geq 0} t\Delta^{-n} H_{F,n})$ suggests that there exists a hierarchy of time scales at which successive orders of the folded model H_F become relevant for the dynamics. These time scales correspond to the powers of the coupling strength Δ . For example, until $t \sim \Delta^k$, at which the prefactor $t\Delta^{-k}$ in front of $H_{F,k}$ becomes appreciable, we expect the dynamics to be governed by the truncation $H^{(k)}$ defined in Eq. (4). This truncation has a set of frozen states that is distinct from those of the higher-order truncations. In particular, some of them are frozen for $H^{(k)}$ but not for $H^{(k+1)}$: they belong to the set $\mathcal{C}_k \setminus \mathcal{C}_{k+1}$, which we refer to as *level* k —see Fig. 2. During the effective time evolution with H , we expect the states in level k not to evolve up to times proportional to Δ^k . At least for large Δ , the same can be expected from the evolution under H_{XPX} , related to H via a unitary transformation e^S —see Eq. (3). Indeed, since the leading order in S is $1/\Delta$, we expect the unitary transformation to be irrelevant at large Δ .

To verify our expectations, we compute how the complexity of level- k frozen states evolves in time under the Hamiltonian H_{XPX} , for various k (see Appendix D for similar results in the quantum Fredrickson-Andersen model). In particular, we consider the *Krylov* (or *spread*) *complexity* which measures the spreading of states through the Hilbert space during time evolution [41, 42]. For any initial state $|\psi\rangle$ it is defined as

$$K_t(\psi) = \sum_{n=0,1,2,\dots} n |\langle \psi(t) | B_n \rangle|^2, \quad (13)$$

where $|\psi(t)\rangle = e^{-itH_{\text{XPX}}} |\psi\rangle$ is the time-evolved state and $\{B_n\}_{n=0,1,2,\dots}$ is the Krylov basis obtained by orthogonalizing the set of states $\{|\psi_n\rangle := (H_{\text{XPX}})^n |\psi\rangle\}_{n=0,1,2,\dots}$.

In Figs. 4(a), (b), (c) we show the time-averaged Krylov complexity $\bar{K}_t(s) := t^{-1} \int_0^t d\tau K_\tau(s)$, additionally averaged over the frozen initial states $|\psi\rangle = |s\rangle$ in different levels of the hierarchy. In particular, the complexity of states in level k remains negligible up to times proportional to Δ^k , after which it exhibits a jump. This is confirmed by the collapse of functions $\bar{K}_t(s)$ in the rescaled time t/Δ^k . Interestingly, we observe that the unitary transformation e^S has little significance even for intermediate values of Δ .

Figures 4(d), (e), (f) demonstrate that the hierarchy of time scales also appears in the correlation functions. While the time-averaged correlations $\bar{c}_t(s) - \bar{c}_\infty(s)$ rapidly decay to zero in nonfrozen states $|s\rangle$ (see Fig. 1), those in level- k frozen states exhibit plateaus that persist up to times proportional to Δ^k . The estimate for the

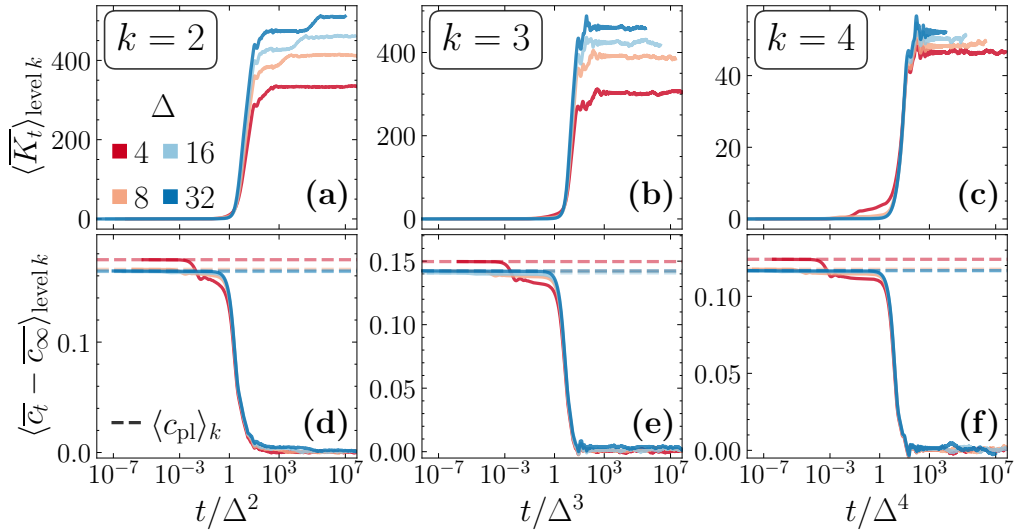


FIG. 4. **Krylov complexity and correlation functions in frozen states.** Panels (a)–(c) show time-averaged Krylov complexity for a level- k initial state, additionally averaged over all initial states in the level. Notice the collapse in the rescaled time t/Δ^k . Panels (d)–(f) show time-averaged correlation functions in level- k states, averaged across the level. The dashed lines show the plateau-height estimates given in Eq. (14). The $O(\Delta^{-2})$ correction in Eq. (14) suggests that the two-staged plateaus (for $\Delta = 4$) become single-staged as $\Delta \rightarrow \infty$. In all plots the system size is $L = 14$.

plateau value of $\overline{c}_t(\mathbf{s})$, derived in Appendix C, reads

$$c_{\text{pl}}(\mathbf{s}) = \frac{N_\uparrow(\mathbf{s})}{L} + O(\Delta^{-2}), \quad (14)$$

where $N_\uparrow(\mathbf{s})$ is the number of \uparrow -spins in the level- k state $|\mathbf{s}\rangle$. As shown in Figs. 4(d), (e), (f), the difference $c_{\text{pl}}(\mathbf{s}) - \overline{c}_\infty(\mathbf{s})$ correctly reproduces the heights of the plateaus. Note that $c_{\text{pl}}(\mathbf{s})$ coincides with the initial value of $\overline{c}_t(\mathbf{s})$ up to an $O(\Delta^{-2})$ correction. The latter arises from the unitary transformation e^S , since the state is evolved with $e^{-itH_{\text{XPX}}} = e^{-S} e^{-itH} e^S$, not with e^{-itH} . Note that some of the plateaus at intermediate values of Δ , shown in Figs. 4(d), (e), (f), are not one- but two-staged on the associated time scale. The $O(\Delta^{-2})$ correction suggests that the second stages in such plateaus disappear as $\Delta \rightarrow \infty$ (plateaus become steps). The above results fully explain the hierarchy of relaxation times depicted in Fig. 1(a).

In general, the decay of correlation functions in level- k frozen states can exhibit a richer structure than in the XPX model discussed above. In particular, it may proceed across multiple time scales $t \sim \Delta^{\ell_j}$, with $\ell_1 < \ell_2 < \dots$ and starting with $\ell_1 = k$. We indeed observe such behavior in the quantum Fredrickson-Andersen model, as reported in Appendix D. This suggests that, during the time evolution, components of the evolving superposition can reenter the nested hierarchy of frozen states, thereby giving rise to additional, longer relaxation time scales.

VI. DISCUSSION

We have traced the emergence of slow relaxation in quantum kinetically constrained models to a nested hierarchy of computational-basis states that remain frozen up to times proportional to the powers of the coupling strength Δ . For the concrete example of the XPX model, our findings are consistent with the observation of spatial heterogeneity in the dynamics, reported in Ref. [31]. Indeed, the times up to which the states in the nested hierarchy remain frozen scale as Δ^k , where k is the smallest spatial separation between spins \downarrow . The latter facilitate the dynamics under the kinetic constraint. We can then expect the regions of space in which \downarrow -spins are further apart to relax exponentially slower than the regions where \downarrow -spins are closer. Crucially, in our case the exponential dependence of time scales on the spatial separation emerges in a clean (unperturbed) system, regardless of its integrability. The underlying mechanism is implicit: it is hidden in the large-coupling expansion, whose higher-order terms in $1/\Delta$ act on progressively larger clusters of spins. In contrast, a broad range of relaxation times can also arise from an explicit perturbation which breaks integrability or constrains the dynamics [46, 47].

Via duality transformations, our results can explain the onset of slow relaxation also in quantum many-body systems in which kinetic constraints are not explicit, but emerge in the large-coupling limit [31, 32]. Whether they can be applied to systems in which kinetic constraints are hard to pinpoint even in the large-coupling limit remains an intriguing open question [48, 49]. Another among open questions concerns the relation be-

tween the nested hierarchy of frozen states and emergent (quasi)conserved quantities [34, 50]. Last but not least, it would be interesting to see whether the nested hierarchy can be extended to include recently discovered Hilbert-space cages [51–54], in addition to frozen states.

Acknowledgements. L.P. is grateful to Urban Duh, Yusuf Kasim, and Pavel Orlov for useful discussions. ED calculations were performed using the QuSpin package [55, 56]. This work has been supported by the Slovenian Research and Innovation Agency (ARIS) under Research Startup Program No. SN-ZRD/22-27/0510—NESY (L.Z. and V.M.) and Research Program No. P1-0402 (L.Z. and L.P.), as well as by the European Research Council (ERC) under Advanced Grant No. 101096208—QUEST (L.Z. and L.P.).

Appendix A: Large-coupling expansion

Here, we report the details for the large-coupling expansion, largely based on Ref. [43]. The starting point is the separation of the Hamiltonian H_{XPX} as

$$H_{\text{XPX}} = H_{\text{F},0} + T_{-1} + T_1 + \Delta V. \quad (\text{A1})$$

Here, $V = \sum_{j=1}^L \sigma_j^z$ is the interaction, whose spectrum is equally spaced. Operators T_m satisfy $[V, T_m] = 4mT_m$ and $T_{-m} \equiv T_m^\dagger$. They cause transitions between the eigenvalues of V that differ by integer multiples of 4. Finally, $H_{\text{F},0}$ is chosen so as to commute with V , i.e., $[V, H_{\text{F},0}] = 0$. In the limit $\Delta \rightarrow \infty$, the transitions between the eigenvalues of ΔV , separated by a multiple of Δ , are prohibitively costly. The leading order of the large coupling expansion is therefore $H_{\text{F},0} + \Delta V$.

Let us introduce compact notation $T_0 \equiv H_{\text{F},0}$ and $T_{m_1, \dots, m_k} \equiv T_{m_1} \dots T_{m_k}$, with $m_j \in \{-1, 0, 1\}$. In this paper we focus on the XPX model, for which T_0 is given in Eq. (5) in the main text, and

$$T_1 = \sum_{j=1}^L \sigma_{j-1}^+ (1 - \sigma_j^z) \sigma_{j+1}^+, \quad (\text{A2})$$

with $\sigma_j^\pm = (\sigma_j^x \pm i\sigma_j^y)/2$. We note, however, that the following discussion works for any Hamiltonian with a separation analogous to Eq. (A1).

The large-coupling expansion consists of anti-Hermitian operators $S^{(n)}$ and effective Hamiltonians $H^{(n)}$, for $n = 1, 2, \dots$, such that

$$e^{S^{(n)}} H_{\text{XPX}} e^{-S^{(n)}} = H^{(n)} + O(\Delta^{-n}) \quad (\text{A3})$$

as $\Delta \rightarrow \infty$, and the effective Hamiltonians $H^{(n)}$ conserve V , i.e., $[H^{(n)}, V] = 0$. Consistently with numerical observations, we will regard the expansion obtained as $n \rightarrow \infty$ not only as asymptotic in Δ , but as a convergent power series. Before proceeding, note that

$$[V, T_{m_1, \dots, m_k}] = \left(4 \sum_{j=1}^k m_j \right) T_{m_1, \dots, m_k}. \quad (\text{A4})$$

Thus, if $\sum_{j=1}^k m_j = 0$, the commutator is zero. In particular, the effective Hamiltonians will be linear combinations of terms T_{m_1, \dots, m_k} with $\sum_{j=1}^k m_j = 0$, while $S^{(k)}$ will consist of such terms with $\sum_{j=1}^k m_j \neq 0$.

The recursive scheme for the large-coupling expansion is now as follows [43]:

1. We start with $S^{(1)} = (4\Delta)^{-1}(T_1 - T_{-1})$.

2. From

$$\begin{aligned} e^{S^{(k)}} H_{\text{XPX}} e^{-S^{(k)}} &= H^{(k)} \\ &+ \Delta^{-k} \sum_{\substack{m_1, \dots, m_{k+1} \\ \in \{-1, 0, 1\}}} C_{m_1, \dots, m_{k+1}} T_{m_1, \dots, m_{k+1}} \\ &+ O(\Delta^{-(k+1)}) \end{aligned} \quad (\text{A5})$$

we obtain $H^{(k)}$, consisting of terms of orders $\Delta, \Delta^0, \dots, \Delta^{1-k}$, as well as the coefficients $C_{m_1, \dots, m_{k+1}}$ describing the correction of order Δ^{-k} .

3. We construct

$$S^{(k+1)} = S^{(k)}$$

$$+ \Delta^{-(k+1)} \sum_{\substack{m_1, \dots, m_{k+1} \\ \sum_{j=1}^{k+1} m_j \neq 0}} \frac{C_{m_1, \dots, m_{k+1}}}{4 \sum_{j=1}^{k+1} m_j} T_{m_1, \dots, m_{k+1}}, \quad (\text{A6})$$

and repeat the steps recursively. In particular, this yields

$$H^{(k+1)} = H^{(k)}$$

$$+ \Delta^{-k} \sum_{\substack{m_1, \dots, m_{k+1} \\ \sum_{j=1}^{k+1} m_j = 0}} C_{m_1, \dots, m_{k+1}} T_{m_1, \dots, m_{k+1}}. \quad (\text{A7})$$

For obtaining the coefficients in the second step of the recurrence, it is convenient to use the Campbell identity

$$e^{S^{(k)}} H_{\text{XPX}} e^{-S^{(k)}} = \sum_{\ell=0}^{k+1} \frac{(\text{ad}_{S^{(k)}})^\ell}{\ell!} H_{\text{XPX}} + O(\Delta^{-k-1}), \quad (\text{A8})$$

where $\text{ad}_X Y := [X, Y]$.

We will write the effective Hamiltonians (i.e., truncations of the expansion in $1/\Delta$) in the form $H^{(k)} = \Delta V + \sum_{n=0}^{k-1} \Delta^{-n} H_{\text{F},n}$ and the generator of the unitary transformation as $S^{(k)} = \sum_{n=1}^k \Delta^{-n} S_n$ —see Eq. (4) in the main text. In this notation, $H_{\text{F}} \equiv \sum_{n=0}^{\infty} \Delta^{-n} H_{\text{F},n}$ is the folded model. Different orders of the expansion are obtained using symbolic programming. The lowest orders (aside from $H_{\text{F},0} \equiv T_0$) read

$$\begin{aligned} H_{\text{F},1} &= \frac{1}{4} [T_{1,-1} - T_{-1,1}], \\ H_{\text{F},2} &= \frac{1}{4^2} [T_{-1,0,1} - \frac{1}{2} T_{-1,1,0} - \frac{1}{2} T_{0,-1,1} - \frac{1}{2} T_{0,1,-1} \\ &\quad - \frac{1}{2} T_{1,-1,0} + T_{1,0,-1}], \\ H_{\text{F},3} &= \frac{1}{4^3} [-\frac{1}{2} T_{-1,-1,1,1} - T_{-1,0,0,1} + T_{-1,0,1,0} + T_{-1,1,-1,1} \\ &\quad - \frac{1}{2} T_{-1,1,0,0} + T_{0,-1,0,1} - \frac{1}{2} T_{0,0,-1,1} + \frac{1}{2} T_{0,0,1,-1} \\ &\quad - T_{0,1,0,-1} + \frac{1}{2} T_{1,-1,0,0} - T_{1,-1,1,-1} - T_{1,0,-1,0} \\ &\quad + T_{1,0,0,-1} + \frac{1}{2} T_{1,1,-1,-1}], \end{aligned} \quad (\text{A9})$$

and

$$\begin{aligned} S_1 &= \frac{1}{4} [T_1 - T_{-1}], \\ S_2 &= \frac{1}{4^2} [T_{-1,0} - T_{0,-1} - T_{0,1} + T_{1,0}], \\ S_3 &= \frac{1}{4^3} \left[\frac{1}{4} T_{-1,-1,0} - \frac{2}{3} T_{-1,-1,1} - \frac{1}{2} T_{-1,0,-1} - T_{-1,0,0} \right. \\ &\quad \left. + \frac{4}{3} T_{-1,1,-1} + \frac{2}{3} T_{-1,1,1} + \frac{1}{4} T_{0,-1,-1} + 2T_{0,-1,0} - \frac{1}{4} T_{1,1,0} \right. \\ &\quad \left. - T_{0,0,-1} + T_{0,0,1} - 2T_{0,1,0} - \frac{1}{4} T_{0,1,1} - \frac{2}{3} T_{1,-1,-1} \right. \\ &\quad \left. + T_{1,0,0} - \frac{4}{3} T_{1,-1,1} + \frac{1}{2} T_{1,0,1} + \frac{2}{3} T_{1,1,-1} \right]. \end{aligned} \quad (\text{A10})$$

By construction, the introduced large-coupling expansion is asymptotic as $\Delta \rightarrow \infty$ [see Eq. (A3)]. However, it seems also to be convergent in k for fixed $\Delta > 1$. Some evidence is presented in Fig. 5.

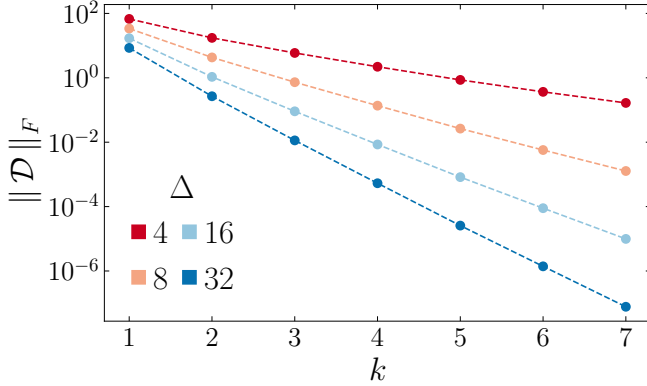


FIG. 5. Convergence of the large-coupling expansion. Frobenius norm of the difference $\mathcal{D} = H_{\text{XPX}} - e^{-S^{(k)}} H^{(k)} e^{S^{(k)}}$ as a function of the truncation order k , for different $\Delta > 1$. System size is $L = 12$.

Appendix B: Counting the frozen states

Here, we compute the size of the set \mathcal{C}_k , which contains the frozen states of $H^{(k)}$. We assume that the system size L is larger than the number of neighboring sites on which the local terms in $H^{(k)}$ act: $L > 2k + 1$. According to our conjecture, any two \downarrow -spins in a state that belongs to \mathcal{C}_k should be separated by at least k spins \uparrow . We start by counting such states at a fixed total number N of \uparrow -spins ($L - N$ is then the number of \downarrow -spins).

Step 1. First consider the blocks of spins

$$A := \underbrace{\downarrow \uparrow \dots \uparrow}_k, \quad B := \uparrow. \quad (\text{B1})$$

We can arrange spins into $N_A := L - N$ blocks A and $N_B := N - k(L - N)$ blocks B . From here, we can already deduce the possible values of the total number of \uparrow -spins, N : since the minimal number of B -s is $N_B^{(\min)} = 0$, we have $\lceil kL/(k+1) \rceil \leq N \leq L$. We can concatenate A -s and B -s in

$$\binom{N_A + N_B}{N_A} = \binom{L - k(L - N)}{L - N} \quad (\text{B2})$$

different ways. Because of the way we arranged spins into the block A , the configurations obtained in this way end in k or more \uparrow -spins on the right-hand side (RHS). We now have to count the rest of configurations—those that end in less than k \uparrow -spins on the RHS.

Step 2. Let us fix the rightmost block to be A , remove $\ell \in \{1, \dots, k\}$ of the rightmost \uparrow -spins in it, and move them to the left-hand side. We obtain

$$\underbrace{\uparrow \dots \uparrow}_\ell \mid \dots A \dots B \dots \mid \underbrace{\downarrow \uparrow \dots \uparrow}_{k-\ell}, \quad (\text{B3})$$

where we have to concatenate $N_A - 1$ remaining blocks A and N_B blocks B in the middle. There are

$$\binom{N_A - 1 + N_B}{N_A - 1} = \binom{L - k(L - N) - 1}{L - N - 1} \quad (\text{B4})$$

such concatenations. Since ℓ can run from 1 to k , we therefore gain

$$k \binom{L - k(L - N) - 1}{L - N - 1} \quad (\text{B5})$$

additional configurations in this way. The total number of frozen states in \mathcal{C}_k that have N \uparrow -spins is now the sum of contributions in Eqs. (B2) and (B5):

$$\begin{aligned} \binom{L - k(L - N)}{L - N} + k \binom{L - k(L - N) - 1}{L - N - 1} &= \\ = \frac{L}{kN - (k-1)L} \binom{kN - (k-1)L}{L - N}. \end{aligned} \quad (\text{B6})$$

The above results generalize (and agree with) the results obtained in Ref. [15]—see Eqs. (56) and (64) therein. Summing over all possible values of N , and adding 1 to account also for the trivial frozen state $|\downarrow\downarrow \dots \downarrow\rangle$, we obtain $|\mathcal{C}_k|$, reported in Eq. (11) in the main text.

Let us now assume that the asymptotic contribution to Eq. (11) in the main text comes from the dominant term in the sum. The latter has the form given in Eq. (B6), for some N which we will find by maximization. We expect $|\mathcal{C}_k|$ to scale exponentially with L and consider the logarithm of Eq. (B6), which has two terms,

$$\log \frac{L}{kN - (k-1)L} + \log \binom{kN - (k-1)L}{L - N}. \quad (\text{B7})$$

The second one scales linearly with L , while the first one represents a logarithmic correction which we will neglect. We then set $N = \rho L$, use Stirling's approximation for $\log \binom{L^{1-k(1-\rho)}}{L(1-\rho)}$, and maximize with respect to ρ . This leads to

$$|\mathcal{C}_k| \sim \left\{ \frac{[1 - k(1 - \rho_k)]^{1-k(1-\rho_k)}}{[(1-\rho_k)^{1-\rho_k} [1 - (k+1)(1-\rho_k)]^{1-(k+1)(1-\rho_k)}]} \right\}^L, \quad (\text{B8})$$

where ρ_k is the solution of

$$(1-\rho) \frac{[1-k(1-\rho)]^k}{[1-(k+1)(1-\rho)]^{k+1}} = 1. \quad (\text{B9})$$

Using this constraint we can further simplify Eq. (B8). In particular, defining

$$\chi_k := \frac{1-k(1-\rho_k)}{1-(k+1)(1-\rho_k)}, \quad (\text{B10})$$

Eq. (B8) becomes $|\mathcal{C}_k| \sim \chi_k^L$ [Eq. (12) in the main text] while Eq. (B9) translates into the constraint $\chi^k(\chi-1) = 1$ satisfied by χ_k .

Appendix C: Plateau values of the correlation functions

Here, we estimate the plateau value of the correlation function $\overline{c}_t(\mathbf{s})$, evaluated in a level- k frozen state, $|\mathbf{s}\rangle \in \mathcal{C}_k \setminus \mathcal{C}_{k+1}$. We first recall that the dynamics on time scales $t \sim \Delta^k$, on which the plateau appears, is governed by $e^{-S} e^{-itH^{(k)}} e^S$. At larger times, higher orders of the effective Hamiltonian kick in and cause the eventual decay of the plateau. In their absence, the correlation function $\overline{c}_t(\mathbf{s})$ would retain its plateau value forever. The plateau height, denoted by $c_{\text{pl}}(\mathbf{s})$, should therefore be equal to the $t \rightarrow \infty$ limit of the correlation function evolved under $e^{-S} e^{-itH^{(k)}} e^S$. We have

$$c_{\text{pl}}(\mathbf{s}) = \sum_{j=1}^L \frac{\delta_{\uparrow,s_j}}{L} \lim_{t \rightarrow \infty} \frac{1}{t} \int_0^t d\tau \langle \psi_{\mathbf{s}}(\tau) | e^S n_j e^{-S} | \psi_{\mathbf{s}}(\tau) \rangle, \quad (\text{C1})$$

where we have defined $|\psi_{\mathbf{s}}(\tau)\rangle := e^{-i\tau H^{(k)}} e^S |\mathbf{s}\rangle$ and used that n_j is diagonal in the computational basis, $\langle \mathbf{s} | n_j | \mathbf{s} \rangle = \delta_{\uparrow,s_j}$. To simplify the time average in Eq. (C1), we now choose a basis $\{|E_{\ell}\rangle\}$, such that $H^{(k)} |E_{\ell}\rangle = E_{\ell} |E_{\ell}\rangle$ and $V |E_{\ell}\rangle = v_{\ell} |E_{\ell}\rangle$: this is possible since $[H^{(k)}, V] = 0$. We obtain

$$\begin{aligned} & \lim_{t \rightarrow \infty} \frac{1}{t} \int_0^t d\tau \langle \psi_{\mathbf{s}}(\tau) | e^S n_j e^{-S} | \psi_{\mathbf{s}}(\tau) \rangle = \\ &= \sum_{E_{\ell}=E_m} \langle \mathbf{s} | e^{-S} |E_{\ell}\rangle \langle E_{\ell}| e^S n_j e^{-S} |E_m\rangle \langle E_m| e^S | \mathbf{s} \rangle = \\ &= \sum_{E_{\ell}=E_m} \langle \mathbf{s} | E_{\ell} \rangle \langle E_{\ell}| n_j |E_m\rangle \langle E_m| \mathbf{s} \rangle + O(\Delta^{-2}). \end{aligned} \quad (\text{C2})$$

In passing to the third row, we have used the Campbell identity

$$e^{-S} |E_{\ell}\rangle \langle E_{\ell}| e^S = |E_{\ell}\rangle \langle E_{\ell}| - \Delta^{-1} [S_1, |E_{\ell}\rangle \langle E_{\ell}|] + O(\Delta^{-2}). \quad (\text{C3})$$

When plugged in Eq. (C2), the first order in $1/\Delta$ disappears, since $\langle \mathbf{s} | [S_1, |E_{\ell}\rangle \langle E_{\ell}|] n_j |E_m\rangle \langle E_m| \mathbf{s} \rangle = 0$. This is

because n_j and $|E_{\ell}\rangle \langle E_{\ell}|$ preserve the magnetization V , while S_1 changes it—see Eq. (8) in the main text. We now note that

$$\begin{aligned} & \sum_{E_{\ell}=E_m} \langle \mathbf{s} | E_{\ell} \rangle \langle E_{\ell}| n_j |E_m\rangle \langle E_m| \mathbf{s} \rangle = \\ &= \lim_{t \rightarrow \infty} \frac{1}{t} \int_0^t d\tau \langle \mathbf{s} | e^{i\tau H^{(k)}} n_j e^{-i\tau H^{(k)}} | \mathbf{s} \rangle = \langle \mathbf{s} | n_j | \mathbf{s} \rangle, \end{aligned} \quad (\text{C4})$$

where we have used that $|\mathbf{s}\rangle \in \mathcal{C}_k \setminus \mathcal{C}_{k+1}$ remains frozen under $H^{(k)}$. Equation (C1) thus simplifies into

$$c_{\text{pl}}(\mathbf{s}) = \sum_{j=1}^L \frac{\delta_{\uparrow,s_j}}{L} + O(\Delta^{-2}), \quad (\text{C5})$$

which is Eq. (14) in the main text.

Appendix D: Quantum Fredrickson-Andersen model

The quantum version of the Fredrickson-Andersen (FA) model [2, 3] reads

$$H_{\text{FA}} = \sum_{j=1}^L n_{j-1} \left\{ \sqrt{c(1-c)} \sigma_j^x - e^s [c(1-n_j) + (1-c)n_j] \right\}, \quad (\text{D1})$$

where $s \in \mathbb{R}$ is the potential energy strength and $c \in (0, 1)$ is an additional parameter. We will restrict to the special point $c = 2/3$, where the model becomes

$$H_{\text{FA}} = \frac{1}{3} \sum_{j=1}^L (n_{j-1} + n_{j+1}) \left[\sqrt{2} \sigma_j^x - e^s (2 - n_j) \right]. \quad (\text{D2})$$

The stochastic point separating the active and inactive regimes is $s = \log \sqrt{2}$.

The large-coupling expansion can be applied with no additional considerations apart for the starting point:

$$H_{\text{FA}} = H_{\text{F},0} + T_{-1} + T_1 + \Delta V, \quad (\text{D3})$$

where

$$H_{\text{F},0} = \frac{2\sqrt{2}}{3} \sum_{\ell=1}^L n_{\ell-1} \sigma_{\ell}^x n_{\ell+1}, \quad (\text{D4})$$

$$T_1 = \frac{\sqrt{2}}{6} \sum_{\ell=1}^L (1 - \sigma_{\ell-1}^z \sigma_{\ell+1}^z) \sigma_{\ell}^-, \quad (\text{D5})$$

$$V = 2 \sum_{\ell=1}^L (n_{\ell-1} + n_{\ell+1})(n_{\ell} - 2), \quad (\text{D6})$$

and we denote $\Delta = e^s/6$. Then, Eqs. (A9) and (A10) can be used. Note that $H_{\text{F},0}$ is the PXP model [57, 58].

In Fig. 6 we present the time evolution of Krylov complexity and correlation functions for the lowest nonempty levels in the hierarchy of states. Similar to the XXP

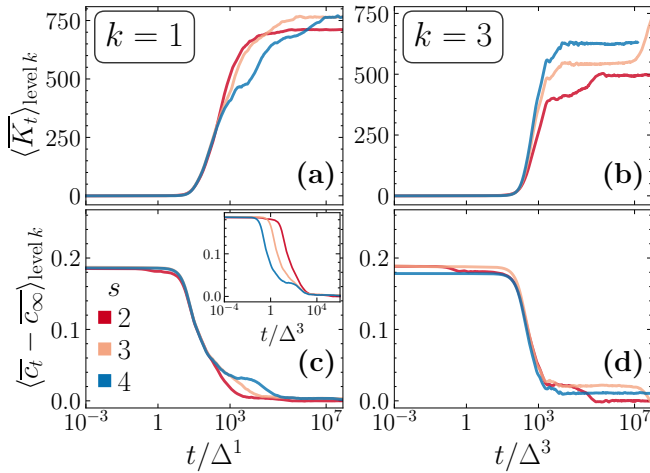


FIG. 6. **Krylov complexity and correlations in frozen states for the quantum FA model.** Panels (a) and (b) show time-averaged Krylov complexity for a level- k initial state, for $k = 1, 3$, additionally averaged over all initial states in the level. Notice the collapse in the rescaled time t/Δ^k , where $\Delta = e^s/6$. Panels (c) and (d) show time-averaged correlation functions $\bar{c}_t(s) = t^{-1} \int_0^t d\tau c_\tau(s)$, Eq. (2) in the main text, in level- k states, averaged across the level. The states in level $k = 1$ have secondary plateaus that collapse in the rescaled time t/Δ^3 , as shown in the inset of panel (c). This indicates that, for times larger than $t \sim \Delta$, such states evolve into a superposition which includes frozen states belonging to level $k = 3$. Levels $k = 2, 4$ in this model are empty, so we omit them. In both plots the system size is $L = 12$.

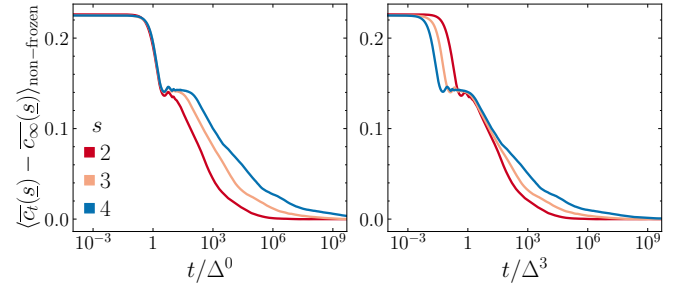


FIG. 7. **Correlations in nonfrozen states for the quantum FA model.** Correlation functions, averaged over all nonfrozen states, are plotted for various values of $\Delta = e^s/6$, in two different time scales: t/Δ^0 and t/Δ^3 .

model discussed in the main text, we observe a collapse in the rescaled time t/Δ^k . Contrary to the XPX model, however, the relaxation of correlation functions in the quantum FA model is multi-staged even for larger values of Δ . For example, for initial states in the level $k = 1$, we observe a secondary plateau with a characteristic time scale $t \sim \Delta^3$, as evident in the inset of Fig. 6(c). A similar two-staged relaxation also appears for correlations in nonfrozen states, as depicted in Fig. 7. The time scales associated with different relaxation stages suggest that initial states $|\psi\rangle$ evolve into superpositions that include frozen states within higher levels of the nested hierarchy, which relax on longer time scales.

[1] R. G. Palmer, D. L. Stein, E. Abrahams, and P. W. Anderson, Models of hierarchically constrained dynamics for glassy relaxation, *Phys. Rev. Lett.* **53**, 958 (1984).

[2] G. H. Fredrickson and H. C. Andersen, Kinetic Ising model of the glass transition, *Phys. Rev. Lett.* **53**, 1244 (1984).

[3] F. Ritort and P. Sollich, Glassy dynamics of kinetically constrained models, *Advances in Physics* **52**, 219 (2003).

[4] J. P. Garrahan, Aspects of non-equilibrium in classical and quantum systems: Slow relaxation and glasses, dynamical large deviations, quantum non-ergodicity, and open quantum dynamics, *Physica A* **504**, 130 (2018).

[5] E. Urban, T. A. Johnson, T. Henage, L. Isenhower, D. D. Yavuz, T. G. Walker, and M. Saffman, Observation of Rydberg blockade between two atoms, *Nature Physics* **5**, 110–114 (2009).

[6] I. Lesanovsky, Many-body spin interactions and the ground state of a dense Rydberg lattice gas, *Phys. Rev. Lett.* **106**, 025301 (2011).

[7] I. Lesanovsky and J. P. Garrahan, Kinetic constraints, hierarchical relaxation, and onset of glassiness in strongly interacting and dissipative Rydberg gases, *Phys. Rev. Lett.* **111**, 215305 (2013).

[8] H. Bernien, S. Schwartz, A. Keesling, H. Levine, A. Omran, H. Pichler, S. Choi, A. S. Zibrov, M. Endres, M. Greiner, V. Vuletić, and M. D. Lukin, Probing many-body dynamics on a 51-atom quantum simulator, *Nature* **551**, 579 (2017).

[9] D. Bluvstein, A. Omran, H. Levine, A. Keesling, G. Semeghini, S. Ebadi, T. T. Wang, A. A. Michailidis, N. Maskara, W. W. Ho, S. Choi, M. Serbyn, M. Greiner, V. Vuletić, and M. D. Lukin, Controlling quantum many-body dynamics in driven Rydberg atom arrays, *Science* **371**, 1355 (2021).

[10] K. Kim, F. Yang, K. Mølmer, and J. Ahn, Realization of an Extremely Anisotropic Heisenberg Magnet in Rydberg Atom Arrays, *Phys. Rev. X* **14**, 011025 (2024).

[11] F. Yang, H. Yarloo, H.-C. Zhang, K. Mølmer, and A. E. B. Nielsen, Probing Hilbert space fragmentation with strongly interacting Rydberg atoms, *Phys. Rev. B* **111**, 144313 (2025).

[12] L. Corcoran, M. de Leeuw, and B. Pozsgay, Integrable models on Rydberg atom chains, *SciPost Phys.* **18**, 139 (2025).

[13] Z.-C. Yang, F. Liu, A. V. Gorshkov, and T. Iadecola, Hilbert-space fragmentation from strict confinement, *Phys. Rev. Lett.* **124**, 207602 (2020).

[14] C. M. Langlett and S. Xu, Hilbert space fragmentation and exact scars of generalized Fredkin spin chains, *Phys. Rev. B* **103**, L220304 (2021).

[15] L. Zadnik and M. Fagotti, The folded spin-1/2 XXZ model: I. Diagonalisation, jamming, and ground state properties, *SciPost Phys. Core* **4**, 010 (2021).

[16] B. Pozsgay, T. Gombor, A. Hutsalyuk, Y. Jiang,

L. Pristyák, and E. Vernier, Integrable spin chain with Hilbert space fragmentation and solvable real-time dynamics, *Phys. Rev. E* **104**, 044106 (2021).

[17] K. Tamura and H. Katsura, Quantum many-body scars of spinless fermions with density-assisted hopping in higher dimensions, *Phys. Rev. B* **106**, 144306 (2022).

[18] A. Kerschbaumer, M. Ljubotina, M. Serbyn, and J.-Y. Desaules, Quantum many-body scars beyond the PXP model in Rydberg simulators, *Phys. Rev. Lett.* **134**, 160401 (2025).

[19] S. Moudgalya, B. A. Bernevig, and N. Regnault, Quantum many-body scars and Hilbert space fragmentation: a review of exact results, *Reports on Progress in Physics* **85**, 086501 (2022).

[20] M. Serbyn, D. A. Abanin, and Z. Papić, Quantum many-body scars and weak breaking of ergodicity, *Nature Physics* **17**, 675 (2021).

[21] F. M. Surace, M. Votto, E. G. Lazo, A. Silva, M. Dalmonte, and G. Giudici, Exact many-body scars and their stability in constrained quantum chains, *Phys. Rev. B* **103**, 104302 (2021).

[22] H. Singh, B. A. Ware, R. Vasseur, and A. J. Friedman, Subdiffusion and many-body quantum chaos with kinetic constraints, *Phys. Rev. Lett.* **127**, 230602 (2021).

[23] Z.-C. Yang, Distinction between transport and Rényi entropy growth in kinetically constrained models, *Phys. Rev. B* **106**, L220303 (2022).

[24] C. McCarthy, H. Singh, S. Gopalakrishnan, and R. Vasseur, Subdiffusive transport in the Fredkin dynamical universality class, *Phys. Rev. B* **111**, 184317 (2025).

[25] D. S. Bhakuni, R. Verdel, J.-Y. Desaules, M. Serbyn, M. Ljubotina, and M. Dalmonte, Anomalously fast transport in non-integrable lattice gauge theories, [arXiv:2509.08889 \[cond-mat.quant-gas\]](https://arxiv.org/abs/2509.08889) (2025).

[26] M. van Horssen, E. Levi, and J. P. Garrahan, Dynamics of many-body localization in a translation-invariant quantum glass model, *Phys. Rev. B* **92**, 100305 (2015).

[27] Z. Lan, M. van Horssen, S. Powell, and J. P. Garrahan, Quantum slow relaxation and metastability due to dynamical constraints, *Phys. Rev. Lett.* **121**, 040603 (2018).

[28] J. Feldmeier, F. Pollmann, and M. Knap, Emergent glassy dynamics in a quantum dimer model, *Phys. Rev. Lett.* **123**, 040601 (2019).

[29] S. Roy and A. Lazarides, Strong ergodicity breaking due to local constraints in a quantum system, *Phys. Rev. Res.* **2**, 023159 (2020).

[30] N. Pancotti, G. Giudice, J. I. Cirac, J. P. Garrahan, and M. C. Bañuls, Quantum east model: Localization, non-thermal eigenstates, and slow dynamics, *Phys. Rev. X* **10**, 021051 (2020).

[31] L. Zadnik and J. P. Garrahan, Slow heterogeneous relaxation due to constraints in dual XXZ models, *Phys. Rev. B* **108**, L100304 (2023).

[32] L. Causer, M. C. Bañuls, and J. P. Garrahan, Nonthermal eigenstates and slow relaxation in quantum Fredkin spin chains, *Phys. Rev. B* **110**, 134322 (2024).

[33] H. G. Menzler, M. C. Bañuls, and F. Heidrich-Meisner, Graph theory and tunable slow dynamics in quantum East Hamiltonians, *Phys. Rev. B* **112**, 115141 (2025).

[34] D. Abanin, W. De Roeck, W. W. Ho, and F. Huveneers, A rigorous theory of many-body prethermalization for periodically driven and closed quantum systems, *Communications in Mathematical Physics* **354**, 809–827 (2017).

[35] M. Fagotti, V. Marić, and L. Zadnik, Nonequilibrium symmetry-protected topological order: Emergence of semilocal Gibbs ensembles, *Phys. Rev. B* **109**, 115117 (2024).

[36] L. Eck and P. Fendley, From the XXZ chain to the integrable Rydberg-blockade ladder via non-invertible duality defects, *SciPost Phys.* **16**, 127 (2024).

[37] W. Cao, Y. Miao, and M. Yamazaki, Global symmetries of quantum lattice models under non-invertible dualities, *SciPost Phys. Core* **8**, 070 (2025).

[38] J. M. Hickey, S. Genway, and J. P. Garrahan, Signatures of many-body localisation in a system without disorder and the relation to a glass transition, *Journal of Statistical Mechanics: Theory and Experiment* **2016**, 054047 (2016).

[39] M. Fagotti, On conservation laws, relaxation and pre-relaxation after a quantum quench, *Journal of Statistical Mechanics: Theory and Experiment* **2014**, P03016 (2014).

[40] L. Zadnik, K. Bidzhiev, and M. Fagotti, The folded spin-1/2 XXZ model: II. Thermodynamics and hydrodynamics with a minimal set of charges, *SciPost Phys.* **10**, 099 (2021).

[41] V. Balasubramanian, P. Caputa, J. M. Magan, and Q. Wu, Quantum chaos and the complexity of spread of states, *Phys. Rev. D* **106**, 046007 (2022).

[42] P. Nandy, A. S. Matsoukas-Roubeas, P. Martínez-Azcona, A. Dymarsky, and A. del Campo, Quantum dynamics in Krylov space: Methods and applications, *Physics Reports* **1125-1128**, 1 (2025), Quantum dynamics in Krylov space: Methods and applications.

[43] A. H. MacDonald, S. M. Girvin, and D. Yoshioka, $\frac{t}{U}$ expansion for the Hubbard model, *Phys. Rev. B* **37**, 9753 (1988).

[44] K. Bidzhiev, M. Fagotti, and L. Zadnik, Macroscopic effects of localized measurements in jammed states of quantum spin chains, *Phys. Rev. Lett.* **128**, 130603 (2022).

[45] L. Zadnik, S. Bocini, K. Bidzhiev, and M. Fagotti, Measurement catastrophe and ballistic spread of charge density with vanishing current, *Journal of Physics A: Mathematical and Theoretical* **55**, 474001 (2022).

[46] A. A. Michailidis, M. Žnidarič, M. Medvedyeva, D. A. Abanin, T. Prosen, and Z. Papić, Slow dynamics in translation-invariant quantum lattice models, *Phys. Rev. B* **97**, 104307 (2018).

[47] M. Lisiecki, J. Bonča, M. Mierzejewski, J. Herbrych, and P. Lydžba, Tunable Hilbert space fragmentation and extended critical regime, *Phys. Rev. B* **112**, 195116 (2025).

[48] G. Carleo, F. Becca, M. Schiró, and M. Fabrizio, Localization and glassy dynamics of many-body quantum systems, *Scientific Reports* **2**, 243 (2012).

[49] K. Honda, Y. Takasu, S. Goto, H. Kazuta, M. Kunimi, I. Danshita, and Y. Takahashi, Observation of slow relaxation due to Hilbert space fragmentation in strongly interacting Bose-Hubbard chains, *Science Advances* **11**, eadv3255 (2025).

[50] I.-C. Chen and T. Iadecola, Emergent symmetries and slow quantum dynamics in a Rydberg-atom chain with confinement, *Phys. Rev. B* **103**, 214304 (2021).

[51] T.-L. Tan and Y.-P. Huang, Interference-caged quantum many-body scars: The Fock space topological localization and interference zeros (2025), [arXiv:2504.07780 \[cond-mat.str-el\]](https://arxiv.org/abs/2504.07780).

[52] T. Ben-Ami, M. Heyl, and R. Moessner, Many-body

cages: Disorder-free glassiness from flat bands in Fock space, and many-body Rabi oscillations (2025), arXiv:2504.13086 [cond-mat.quant-gas].

[53] E. Nicolau, M. Ljubotina, and M. Serbyn, Fragmentation, zero modes, and collective bound states in constrained models (2025), arXiv:2504.17627 [quant-ph].

[54] C. Jonay and F. Pollmann, Localized Fock space cages in kinetically constrained models (2025), arXiv:2504.20987 [quant-ph].

[55] P. Weinberg and M. Bukov, QuSpin: A Python package for dynamics and exact diagonalisation of quantum many body systems. Part I: Spin chains, *SciPost Phys.* **2**, 003 (2017).

[56] P. Weinberg and M. Bukov, QuSpin: A Python package for dynamics and exact diagonalisation of quantum many body systems. Part II: Bosons, fermions and higher spins, *SciPost Phys.* **7**, 020 (2019).

[57] I. Lesanovsky and H. Katsura, Interacting Fibonacci anyons in a Rydberg gas, *Phys. Rev. A* **86**, 041601 (2012).

[58] C. J. Turner, A. A. Michailidis, D. A. Abanin, M. Serbyn, and Z. Papić, Weak ergodicity breaking from quantum many-body scars, *Nature Physics* **14**, 745 (2018).